Check for updates

## **QUANTUM PROCESSING**

# Quantum learning advantage on a scalable photonic platform

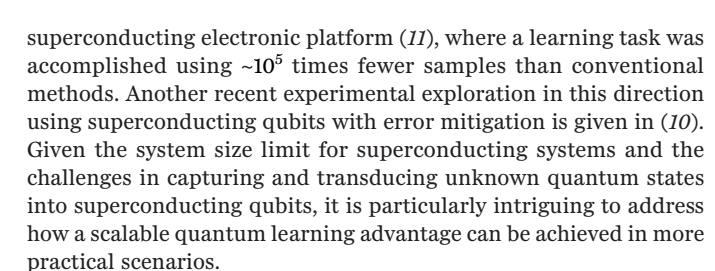
Zheng-Hao Liu<sup>1</sup>\*†, Romain Brunel<sup>1</sup>†, Emil E. B. Østergaard<sup>1</sup>, Oscar Cordero<sup>1</sup>, Senrui Chen<sup>2</sup>, Yat Wong<sup>2</sup>, Jens A. H. Nielsen<sup>1</sup>, Axel B. Bregnsbo<sup>1</sup>, Sisi Zhou<sup>3,4,5</sup>, Hsin-Yuan Huang<sup>6,7,8</sup>, Changhun Oh<sup>9</sup>, Liang Jiang<sup>2</sup>, John Preskill<sup>7</sup>, Jonas S. Neergaard-Nielsen<sup>1</sup>, Ulrik L. Andersen<sup>1</sup>\*

Recent advances in quantum technologies have demonstrated that quantum systems can outperform classical ones in specific tasks, a concept known as quantum advantage. Although previous efforts have focused on computational speedups, a definitive and provable quantum advantage that is unattainable by any classical system has remained elusive. In this work, we demonstrate a provable photonic quantum advantage by implementing a quantum-enhanced protocol for learning a high-dimensional physical process. Using imperfect Einstein-Podolsky-Rosen entanglement, we achieve a sample complexity reduction of 11.8 orders of magnitude compared to classical methods without entanglement. These results show that large-scale, provable quantum advantage is achievable with current photonic technology and represent a key step toward practical quantum-enhanced learning protocols in quantum metrology and machine learning.

Learning the properties of a physical system by performing measurements on it is at the foundation of natural sciences. In conventional settings, this typically involves collecting a large set of independent measurements of certain variables of the system and applying statistical methods on a classical computer to estimate their underlying distribution, from which the properties of the system can be inferred. However, in quantum systems, the learning task is hindered by the constraints of quantum physics, such as the inherent quantum noise associated with measurements, encapsulated by Heisenberg's uncertainty principle. Consequently, the sample complexity—the number of experiments required to learn certain properties of quantum systems—can scale exponentially with the system size, rendering some learning tasks practically infeasible using classical, conventional learning approaches (1, 2).

As an alternative to the conventional approach using independent probe states and a classical processor for data analysis, quantum learning strategies have been proposed (3–5, 6, 7–10). In such approaches, the probe states are not measured independently but instead undergo a collective quantum algorithmic measurement before data analysis is conducted. By leveraging quantum coherence of the probe states and collective measurements, it has been shown that, for certain finite-dimensional quantum systems, the sample complexity can be substantially reduced (3, 9). Building on these ideas, quantum advantage in learning was first demonstrated on a 40-qubit

<sup>1</sup>Center for Macroscopic Quantum States (bigQ), Department of Physics, Technical University of Denmark, Fysikvej, Kongens Lyngby, Denmark. <sup>2</sup>Pritzker School of Molecular Engineering, The University of Chicago, Chicago, IL, USA. <sup>3</sup>Perimeter Institute for Theoretical Physics, Waterloo, Ontario, Canada. <sup>4</sup>Department of Applied Mathematics, University of Waterloo, Waterloo, Ontario, Canada. <sup>5</sup>Department of Physics and Astronomy and Institute for Quantum Computing, University of Waterloo, Waterloo, Ontario, Canada. <sup>6</sup>Google Quantum Al, Venice, CA, USA. <sup>7</sup>Institute for Quantum Information and Matter, California Institute of Technology, Pasadena, CA, USA. <sup>8</sup>Center for Theoretical Physics, Massachusetts Institute of Technology, Cambridge, MA, USA. <sup>9</sup>Department of Physics, Korea Advanced Institute of Science and Technology, Daejeon, Korea. \*\*Corresponding author. Email: zheli@dtu.dk (Z.-H.L.); ulrik. andersen@fysik.dtu.dk (U.L.A.) †These authors contributed equally to this work.



In our work, we advance the frontier of quantum learning by demonstrating an unprecedented quantum advantage, achieving ordersof-magnitude improvement on a scalable continuous-variable (CV) photonic platform. Using imperfect Einstein-Podolsky-Rosen (EPR) entangled states of light and a joint CV measurement approach, we learn the amplitude and phase distributions of a multimode displacement process with 10<sup>11</sup> times fewer samples than required by an approach without entanglement. Furthermore, our photonic platform enables a considerable quantum advantage in distinguishing two families of processes. Our implementation, capable of learning an infinite-dimensional joint displacement process spanning more than 100 modes, tackles problems whose complexity substantially surpasses that of the previous superconducting qubit-based demonstration (11). The photonic CV platform (12) has been at the forefront in advancing quantum technologies—from boson sampling (13, 14) to quantum communication (15-17), computation (18-20), and sensing (21-23). This work demonstrates how photonic systems can be further leveraged to enhance our ability to learn about physical systems. Moreover, although photonic systems have previously demonstrated their potential in various areas of quantum information, a definitive quantum advantage in such systems has remained elusive (24). Our achievement thus represents an important milestone in both quantum learning and the broader field of quantum information science.

## Context

The task of quantum learning proceeds as follows: The experimenter aims to learn a specific property of a quantum system, such as the probability distribution of a quantum state or the noise characteristics of a particular quantum device. The experimenter probes the device N times, yielding N data samples (Fig. 1A), from which the target property or probability distribution is reconstructed with a certain precision or classified with a specified confidence.

In this work, we focus on the task of learning the properties of random *n*-mode phase-space displacement processes, which model the physical process of random amplitude and phase noise in bosonic channels. These channels are of particular interest because any CV noise channel can be tailored into a random displacement channel by twirling with displacement operators, similar to Pauli twirling in discrete-variable (DV) systems (25). Moreover, learning the properties of multi-time displacement processes has broad applications including gravitational-wave detection (26, 27), Raman spectroscopy (28, 29), dark-matter searches (30, 31), and microscopic force sensing (32).

We learn the dynamical displacement process, labeled  $\Lambda$ , by probing it with quantum states of light, followed by measurements that extract information about the probability distribution  $p(\alpha)$  of the n-mode displacement process, where  $\alpha$  is the n-dimensional complex-valued vector describing the phase-space displacement (see supplementary materials section 2.1 for the formal definition of the displacement process). To achieve the highest confidence in detecting extremely small phase-space displacements and their correlations, we need to reconstruct the characteristic function  $\lambda(\beta)$ —the Fourier conjugate of  $p(\alpha)$  defined on the dual space, for large  $|\beta|^2$ . These parts of  $\lambda(\beta)$  encode the fine structure of the displacement channel in its high-frequency components. It was proved that the conventional learning is not effective for this task: In a previous work by some of us (8), we proved that learning  $\lambda(\beta)$  to

Science 25 SEPTEMBER 2025

a fixed accuracy within a hyperball of squared radius  $|\beta|^2 \propto n$  requires a number of samples scaling exponentially in the number of modes n. Here, we extend this result, showing (see supplementary material, Theorem 3) that this classical complexity lower bound persists for multi-time processes and adaptive measurements. The bound holds for any choice of probe state as long as it is not entangled with an external quantum memory.

### **Quantum-enhanced learning**

We use entanglement to overcome this limitation on learning a random displacement process. Our quantum-enhanced learning scheme is illustrated in Fig. 1C. Each probe mode in the probing state is entangled with a corresponding auxiliary memory mode, forming EPR entangled (or two-mode squeezed) states of a certain squeezing level. The learning is performed by sending probe modes through the displacement process and then performing pairwise CV Bell measurements with memory modes. These Bell measurements reveal correlations between amplitude and phase quadratures with a phasespace resolution determined by the amount of entanglement, bypassing the limitation imposed by the uncertainty principle of individual measurements. In supplementary materials section 2.2, we describe the method for estimating the characteristic function from the measured samples.

We realize the quantum-enhanced learning protocol in a CV optical setup, as illustrated in Fig. 1D, with a detailed description provided in supplementary materials section 1. The twomode squeezed vacuum states, comprising the probe and memory modes, are generated by interfering the outputs of two optical parametric oscillators (OPOs). The displacement process is implemented by mixing a weak coherent state into the probe modes via an unbalanced beam splitter (see Fig. 1E). To extract the displacement information, we perform Bell measurements by interfering the probe and memory modes and using homodyne detection to measure the amplitude and phase quadratures of the resulting output signals. Our OPOs achieve up to 68% reduction of noise power during Bell measurements, enabling high precision in detecting the effects of the process.

## **Process reconstruction**

We demonstrate the quantum enhancement of the learning task by reconstructing the characteristic function  $\lambda(\beta)$  of a class of three-peak displacement processes, defined in supplementary materials, Definition 4, using Bell measurement outcomes. We denote the reconstructed characteristic function as  $\tilde{\lambda}(\beta)$ . For a fixed squeezing parameter r, achieving a given reconstruction accuracy requires  $N \sim \exp(2e^{-2r}|\beta|^2)$  samples, which grows exponentially with  $|\beta|^2$ . When the number of samples N is insufficient, the reconstructed characteristic function  $\tilde{\lambda}(\beta)$  can diverge

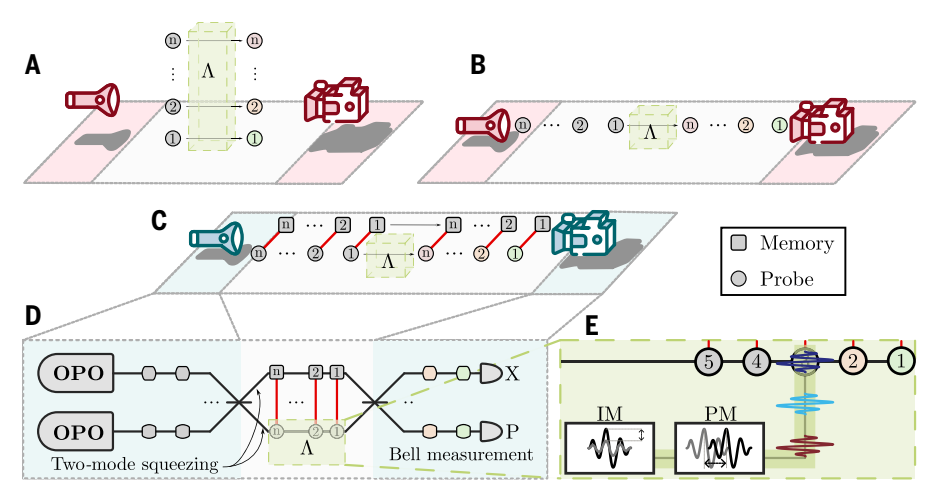
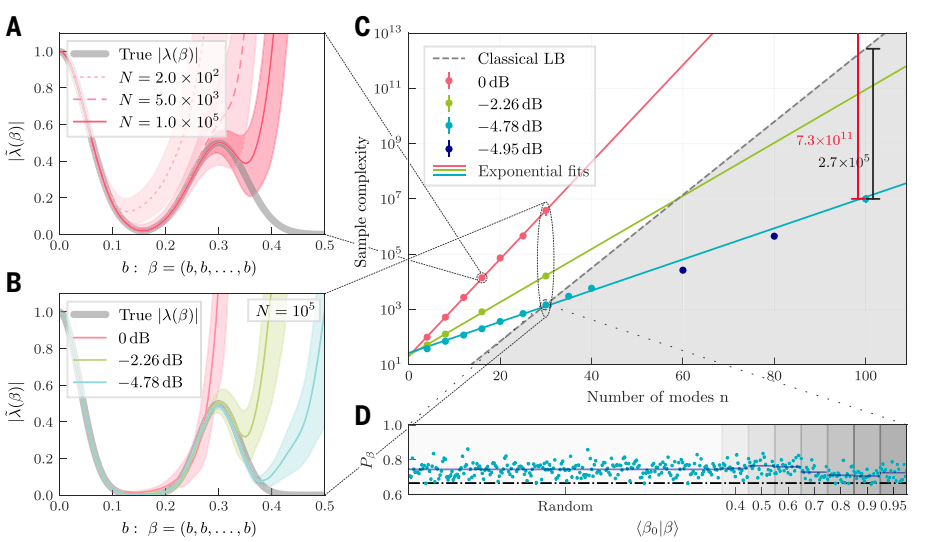


Fig. 1. Quantum entanglement-enhanced learning with photons. (A) Conventional learning of a channel. A multimode probe state is sent through a channel,  $\Lambda$ , followed by a measurement of the probe state to extract the information about the channel. (B) Conventional learning of a multi-time physical process (also denoted as  $\Lambda$ ), in which the measurement settings are allowed to be adaptive within a sample. (C) Quantum entanglement-enhanced learning of a multi-time process. The probe state is entangled with an external memory state. The joint measurement of both states makes overcoming the classical complexity limit possible. (D) Implementation of quantum learning with squeezed light. Two-mode squeezing is generated using two optical parametric oscillators (OPOs). The two spatial modes are temporally multiplexed and used as the probe and memory state, respectively. A Bell measurement between the corresponding temporal modes extracts the information. (E) We realize the displacement process by mixing a modulated coherent state into the probe. IM (PM) intensity (phase) modulator.



**Fig. 2. Reconstruction of a physical process.** (**A**) Experimentally reconstructed characteristic function  $\tilde{\lambda}(\beta)$  of an n=16-mode three-peak process (defined in supplementary materials, Definition 4) with fixed parameters using entanglement-free strategies, compared with the true characteristic function  $\lambda(\beta)$ . The lines (shadings) show the average outcome ( $1\sigma$  standard deviation) of 100 runs of reconstruction using different numbers of samples. (**B**) Same as (A), but using probe states with different amounts of entanglement. Here the number of modes is n=30, and we always use  $10^5$  samples. (**C**) Required number of samples versus n to  $\epsilon$ -close reconstruct  $\lambda(\beta)$  of the three-peak process along the  $\beta_0$  direction, with  $\epsilon=0.24$  and success probability  $1-\delta=2/3$ . The points are determined from experimental results, and the  $1\sigma$  standard deviation error bars are smaller than the data points. Each solid line is a log-linear fit estimating the sample complexity that uses the indicated amount of squeezing. The gray dashed line is the sample complexity lower bound that applies to any entanglement-free strategy that can learn all processes in a large family, which includes the process that we studied. (**D**) Probability of achieving an  $\epsilon$ -close reconstruction of the -4.78-dB, 30-mode characteristic function for various directions in the dual space. The shading highlights the proximity to the displacement direction  $\beta_0$ . Each probability is computed using N=1472 samples—the same as required for an  $\epsilon$ -close reconstruction in (C). The dashed line indicates the target probability of  $1-\delta$ .

at large  $|\beta|^2$ . To visualize this divergence behavior, we plot the reconstructed characteristic function along a slice  $\beta_0=b$   $(1,1,\ldots,1),b\in[0,0.5]$  in the high-dimensional dual space in Fig. 2A: Without squeezing (r=0), the 16-mode characteristic function reconstructed from 200 samples diverges rapidly and fails to capture the ground truth's peak at b=0.3. Furthermore, extending the radius  $|\beta|$  of the reconstructable hyperball requires a substantial increase in sample complexity:  $\sim 10^5$  samples are needed to reveal the peak at b=0.3.

The introduction of entanglement through two-mode squeezing (r>0) markedly reduces this sample complexity. As shown in Fig. 2B, when the number of modes increases to 30, reconstruction without entanglement (r=0) fails even with  $10^5$  samples, requiring an impractically large number of experiments. However, with moderate entanglement, faithful reconstruction becomes achievable with the same number of samples. To systematically investigate the effect of entanglement on sample complexity across different numbers of modes, we implement various n-mode displacement processes using three distinct squeezing levels: 0 dB, -2.26 dB, and -4.78 dB. We characterize the reconstruction performance using  $(\epsilon, \delta)$ -complexity: the number of samples required to reconstruct  $\lambda(\beta)$  with precision  $\epsilon$ , such that  $|\tilde{\lambda}(\beta) - \lambda(\beta)| < \epsilon$  for all  $|\beta| \le 0.3 \sqrt{n}$ , with success probability  $1 - \delta$ . Further details of the process reconstruction experiment are provided in supplementary materials section 4.

As shown in Fig. 2C, entanglement in the form of two-mode squeezing significantly reduces the sample complexity, leading to substantial quantum advantage as the number of modes increases. For n=100, the sample complexity with the strongest squeezing (-4.78 dB) remains about  $10^7$ . By contrast, from an exponential fit of low-mode number data, we estimate that the entanglement-free scheme using vacuum probe would require a sample complexity as high as  $7.3 \times 10^{18}$ , or more

than 20 million years for acquiring all the data if the samples are generated at the same rate (1 MHz per mode) as in our experiment. This represents an empirical improvement of 11.8 orders of magnitude. Although we used a specific process as an example, we believe the scaling of quantum learning advantage also applies to many other time-correlated displacement processes.

Further, in Fig. 2D, we confirm that the success probability of reconstructing  $\lambda(\beta)$  is the lowest along directions  $\beta$  that are close to  $\beta_0$  i.e., in the direction of the distribution's high-frequency peaks. Therefore, the sample complexity in Fig. 2C is a faithful estimation of the true complexity for learning this channel.

# Provable, scalable quantum advantage

Also shown in Fig. 2C is a lower bound on the sample complexity of entanglement-free learning schemes, derived in supplementary materials section 2.3. Compared to this bound, the entanglementenhanced reconstruction of the 100-mode process uses more than five orders of magnitude fewer samples. However, the sample complexity lower bound applies to entanglement-free schemes that can learn the characteristic function  $\lambda(\beta)$  for any random displacement process in a large family and all values of  $\beta$  in a specified bounded range, whereas our experiment learns the characteristic function for processes chosen from a smaller family and more restricted values of β. Therefore, the above improved process reconstruction does not demonstrate a provable quantum advantage.

To establish a provable quantum advantage, we consider the task of identifying specific features of an unknown process. Specifically, we design

a hypothesis testing game (see Fig. 3A) in which a dealer prepares several n-mode displacement processes  $\Lambda_k$ . Each process may or may not exhibit a feature—specifically, two peaks at the locations  $\pm \gamma_k$  in its characteristic function. The processes with and without the feature are grouped into three-peak and Gaussian families, respectively (see supplementary materials, Definitions 4 and 5). A challenger is allowed to implement each process N times. After all the measurements are finished, the dealer reveals  $\gamma_k$  and the challenger is asked to identify the family that the process belongs to. A challenger using the quantum strategy records the Bell measurement outcomes and computes the estimator  $\tilde{\lambda}(\beta)$  at  $\beta = \gamma_k$  once the value is announced. They then compare the value of  $\tilde{\lambda}(\beta)$ with a threshold  $\lambda_0$  to classify the process. If  $\tilde{\lambda}(\beta) > \lambda_0$  is observed, they will guess the process as three-peak type, and otherwise as Gaussian. Crucially, the random nature of  $\gamma_k$  removes the excessive prior information. Consequently, an experimentally measured sample complexity surpassing the classical complexity bound can demonstrate a provable quantum advantage. However, the quantum strategy remains effective even if the challenger is unaware of  $\gamma_k$  during the measurement process, highlighting the practicality of the approach.

We conducted a series of hypothesis-testing games to conclusively observe the provable quantum advantage, with full details provided in supplementary materials section 4. In these games, the average distance of the peaks from the origin is proportional to  $\sqrt{\kappa n}$ , where the resolution constant  $\kappa=0.2$  controls the hardness of the task. First, we fixed the number of samples at  $N=10^5$  and classified a set of 40-mode processes using different levels of two-mode squeezing. The behavior of the estimators across these experiments is reported in Fig. 3B. As the squeezing increases, the displacement signal becomes more pronounced against the noise, and the estimator distribution evolves from being almost random to strongly

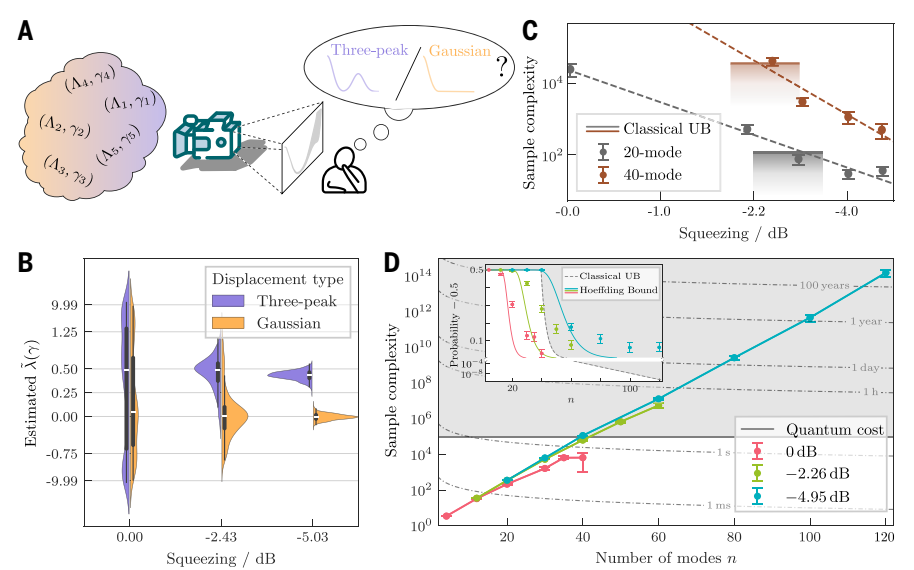


**Fig. 3. Hypothesis testing.** (**A**) The objective is to distinguish whether a displacement process belongs to the three-peak family with unknown parameters or the Gaussian family. (**B**) An example of the separation of the estimator,  $\tilde{\lambda}(\beta = \gamma)$ , for two types of 40-mode displacement processes using different amounts of squeezing. In the noiseless case, the value is expected to be 0.5 (0) for the three-peak (Gaussian) channel. (**C**) Sample complexity for achieving  $^2/3$  success probability in a  $\kappa = 0.2$  hypothesis test using varying amounts of squeezing. The solid and dashed lines indicate the classical complexity bound for achieving the same success probability and the exponential fit, respectively. The shading indicates the existence of a quantum advantage (see supplementary materials section 4.2 for more details). (**D**) Inset: measured probability of winning the hypothesis testing game versus the number of modes, using  $10^5$  samples at various squeezing levels. Solid lines represent pessimistic estimations derived from the Hoeffding bound (8). Main panel: Minimum sample complexity for any conventional strategy to achieve the same success probability as reported in the inset, calculated according to the classical complexity bound, and the corresponding sample collection time at a 1 MHz/mode rate. Error bars represent the  $1\sigma$  standard deviation from a 25-step sequential sampling.

Science 25 SEPTEMBER 2025 1334

clustering around the true value. Next, we used the Monte Carlo method to determine the sample complexity for achieving a success probability of 2/3 in 20-mode and 40-mode hypothesis testing games. As shown in Fig. 3C, squeezing reduces the sample complexity in these tasks. Even at these modest mode numbers, a quantum advantage is clearly observed.

Finally, we explore the scaling of quantum advantage with the number of modes of the displacement process. To do this, we measured the success probability of hypothesis testing with a fixed sample size of  $N = 10^5$ , then calculated the number of classical samples required to achieve the same success probability. A higher success probability corresponds to a larger equivalent classical sample complexity and demonstrates a stronger quantum advantage. As the number of modes increases, process classification becomes more challenging because the estimator diverges for even smaller values of  $\beta$ . This behavior is illustrated in Fig. 3D inset, which shows that the success probability evolves through three phases: starting from  $\simeq 1$  for small n where the information from the displacement process dominates the noise, transitioning through a region of decline, and eventually converging to  $\simeq 0.5$  when noise prevails and the estimator "diverges" at  $\beta = \gamma$ , making the estimate effectively a coin toss. Increased squeezing shifts the transition region to higher mode numbers, allowing some data points to achieve success probability above what is possible with classical strategies using the same number of samples. When the success probability significantly exceeds 0.5, we compute the equivalent classical sample complexity and compare it with the 10<sup>5</sup> realized samples. Our results, shown in Fig. 3D, emphasize how the quantum advantage grows as the number of modes increases. For the largest-scale (120-mode) experiment run across a 12-s effective sampling time at a 1-MHz rate, we measured a success probability of  $0.563 \pm 0.025$ , exceeding the bound for conventional strategy  $(0.5 + 3.8 \times 10^{-11})$  with a confidence level of 99.3%. To achieve the same success probability,  $1.6 \times 10^{14}$ classical samples would be required. This translates into an expected measurement time of more than 600 years. Our result thus indicates a provable quantum advantage of 9.2 orders of magnitude.

#### Outlook

In this work, we have demonstrated a substantial quantum advantage in learning using a scalable, albeit noisy and lossy, photonic platform based on EPR entangled states and CV Bell measurements. Whereas previous demonstrations of quantum advantage have primarily focused on quantum computational tasks such as Gaussian boson sampling, our work demonstrates a substantial quantum advantage in learning. Further, our research sheds light on a new quantum learning framework, where the information is encoded into the temporal domain. This quantum learning framework invites further exploration both in theory and in experiments.

Our method enables the resolution of intricate features in highly complex systems, offering to potentially uncover hidden structures that would remain completely inaccessible with classical techniques and emphasizing the versatility of photonic platforms for advancing quantum technologies. Looking ahead, our results have the potential to drive progress in quantum-enhanced sensing, parameter estimation, and machine learning, for which the photonic platform is well-suited for tackling high-dimensional discrete-variable and continuous-variable problems. We believe that extending the current protocol to more generic processes and introducing adaptive strategies could further strengthen the quantum learning advantages.

### **REFERENCES AND NOTES**

- L. Banchi, J. L. Pereira, S. T. Jose, O. Simeone, Adv. Quantum Technol. 2024, 2300311 (2023)
- 2. A. Anshu, S. Arunachalam, Nat. Rev. Phys. 6, 59-69 (2024).
- 3. H. Y. Huang, R. Kueng, J. Preskill, Phys. Rev. Lett. 126, 190505 (2021).
- D. Aharonov, J. Cotler, X. L. Qi, Nat. Commun. 13, 887 (2022).
- 5. S. Chen, S. Zhou, A. Seif, L. Jiang, *Phys. Rev. A* **105**, 032435 (2022)
- $6..\ \ M.\ C.\ Caro, \textit{ACM Transactions on Quantum Computing}\ \ \textbf{5}, 1-53\ (2024).$

- 7. Z. M. Rossi, J. Yu, I. L. Chuang, S. Sugiura, Phys. Rev. A 105, 032401 (2022).
- 8. C. Oh et al., Phys. Rev. Lett. 133, 230604 (2024).
- S. Chen, J. Cotler, H. Y. Huang, J. Li, in 2021 IEEE 62nd Annual Symposium on Foundations of Computer Science (FOCS) (2022), pp. 574–585 (2022).
- 10. A. Seif et al., arXiv:2408.03376 [quant-ph] (2024).
- 11. H.-Y. Huang et al., Science 376, 1182-1186 (2022).
- 12. C. Weedbrook et al., Rev. Mod. Phys. 84, 621-669 (2012).
- 13. H.-S. Zhong et al., Science 370, 1460-1463 https://www.science.org (2020).
- 14. L. S. Madsen et al., Nature 606, 75-81 (2022).
- 15. M. Takeoka, S. Guha, M. M. Wilde, Nat. Commun. 5, 5235 (2014).
- 16. S. Pirandola, R. Laurenza, C. Ottaviani, L. Banchi, Nat. Commun. 8, 15043 (2017).
- 17. S. Pirandola et al., Adv. Opt. Photonics 12, 1012 (2020).
- M. V. Larsen, X. Guo, C. R. Breum, J. S. Neergaard-Nielsen, U. L. Andersen, Nat. Phys. 17, 1018–1023 (2021).
- 19. I. Tzitrin et al., PRX Quantum 2, 040353 (2021).
- M. V. Larsen, C. Chamberland, K. Noh, J. S. Neergaard-Nielsen, U. L. Andersen, *PRX Quantum* 2, 030325 (2021).
- 21. M. Tse et al., Phys. Rev. Lett. 123, 231107 (2019).
- 22. X. Guo et al., Nat. Phys. 16, 281-284 (2020).
- J. A. H. Nielsen, J. S. Neergaard-Nielsen, T. Gehring, U. L. Andersen, *Phys. Rev. Lett.* 130, 123603 (2023).
- 24. C. Oh, M. Liu, Y. Alexeev, B. Fefferman, L. Jiang, Nat. Phys. 20, 1461–1468 (2024).
- 25. J. J. Wallman, J. Emerson, Phys. Rev. A 94, 052325 (2016).
- 26. D. Ganapathy et al., Phys. Rev. X 13, 041021 (2023).
- 27. C. H. Valahu, T. Navickas, M. J. Biercuk, T. R. Tan, arXiv:2405.15237 [quant-ph] (2024).
- 28. J.-X. Cheng, X. S. Xie, Science 350, aaa8870 (2015).
- 29. R. B. de Andrade et al., Optica 7, 470-475 (2020).
- 30. K. M. Backes et al., Nature 590, 238-242 (2021).
- 31. A. J. Brady et al., PRX Quantum 3, 030333 (2022).
- 32. S. Barzanjeh et al., Nat. Phys. 18, 15-24 (2022).
- R. Brunel, Z.-H. Liu, J. S. Neergaard-Nielsen, Data and code for "Quantum learning advantage on a scalable photonic platform," figshare (2025); https://doi.org/10.11583/ DTU.29517107v1.

#### **ACKNOWLEDGMENTS**

We thank H. Q. Nguyen and B. L. Larsen for helpful feedback on the paper. Funding: Z.-H.L., R.B., E.E.B.Ø., O.C., J.A.H.N., J.S.N.-N., and U.L.A. acknowledge support from the Danish National Research Foundation, Center for Macroscopic Quantum States (bigQ, DNRF0142), EU project CLUSTEC (grant agreement no. 101080173), EU ERC project ClusterQ (grant agreement no. 101055224), NNF project CBQS (NNF 24SA0088433), Innovation Fund Denmark (PhotoQ project, grant no. 1063-00046A), and the MSCA European Postdoctoral Fellowships (GTGBS, project no. 101106833). J.P. acknowledges support from the US Department of Energy, Office of Science, Office of Advanced Scientific Computing Research (DE-NA0003525, DE-SC0020290), the US Department of Energy, Office of Science, National Quantum Information Science Research Centers, Quantum Systems Accelerator, and the National Science Foundation (PHY-1733907). The Institute for Quantum Information and Matter is an NSF Physics Frontiers Center. L.J. acknowledges support from the ARO(W911NF-23-1-0077), ARO MURI (W911NF-21-1-0325), AFOSR MURI (FA9550-19-1-0399, FA9550-21-1-0209, FA9550-23-1-0338), DARPA (HR0011-24-9-0359, HR0011-24-9-0361), NSF (OMA-1936118, ERC-1941583, OMA-2137642, OSI-2326767, CCF-2312755), NTT Research, and the Packard Foundation (2020-71479). S.Z. acknowledges funding provided by Perimeter Institute for Theoretical Physics, a research institute supported in part by the Government of Canada through the Department of Innovation, Science and Economic Development Canada and by the Province of Ontario through the Ministry of Colleges and Universities. C.O. was supported by the National Research Foundation of Korea grants (nos. RS-2024-00431768 and RS-2025-00515456) funded by the Korean government [Ministry of Science and ICT (MSIT)] and the Institute of Information & Communications Technology Planning & Evaluation (IITP) grants funded by the Korea government (MSIT) (nos. IITP-2025-RS-2025-02283189 and IITP-2025-RS-2025-02263264). **Author contributions:** L.J., U.L.A., H.-Y.H., and J.P. conceived the project. S.C. and C.O. developed the theoretical scheme with input from Y.W. and S.Z. J.S.N.-N., J.A.H.N., and Z.-H.L. designed the experiment. Z.-H.L. and R.B. performed the experiment and data analysis. J.A.H.N., O.C., E.E.B.Ø., and R.B. built the squeezing sources, and they built the setup together with Z.-H.L. and A.B.B. J.S.N.-N. and U.L.A. supervised the experiment. U.L.A., Z.-H.L., and R.B. wrote the manuscript with reviewing and editing from all the authors. Competing interests: There are no competing interests to declare. Data and materials availability: All data needed to evaluate the conclusions in the paper are present in the paper. The Bell measurement data that supports the findings of this study, together with the source code for analyzing the data, are available at figshare (33). License information: Copyright @ 2025 the authors, some rights reserved; exclusive licensee American Association for the Advancement of Science. No claim to original US government works. https://www.science.org/about/science-licenses-journal-article-reuse

#### SUPPLEMENTARY MATERIALS

science.org/doi/10.1126/science.adv2560 Supplementary Text; Figs. S1 to S10; Tables S1 to S3; References (34–40); Algorithms S1 and S2

Submitted 27 March 2025; accepted 21 July 2025

10.1126/science.adv2560

1335

Science 25 SEPTEMBER 2025